International Symposium
On Turbulence and Shear Flow
Phenomena (TSFP-8)
August 28 - 30, 2013 Poitiers, France

COMPARISON OF NEAR-FIELD EVENTS AND THEIR FAR-FIELD ACOUSTIC SIGNATURES IN EXPERIMENTAL AND NUMERICAL HIGH SPEED JETS

Pinqing Kan
Syracuse University
pkan@syr.edu

Jacques Lewalle
Syracuse University
jlewalle@syr.edu

Guillaume Daviller
Institut Pprime, Université de Poitiers and Cerfacs, Toulouse
daviller@cerfacs.fr

ABSTRACT

Two different approaches are applied to near-field (NF) velocity field and far-field (FF) pressure signals to gain better understanding of the flow structures that contribute to high speed jet noise. We use laboratory data from a 10kHz TRPIV experiment data of Mach 0.6 jet and numerical data from an 80kHz LES database at Mach 0.9 jet. From the NF, over 20 representative diagnostics are extracted as time traces, of which about half give high correlation with the far-field. Utilizing cross-correlation and wavelet analysis, we locate the frequency band where information is transferred from NF to FF. Furthermore we identify excerpts in time and frequency domain that act as major correlation contributors. The lists of events based on FF only (acoustic footprints) and on NF-FF correlations are compared and show good similarity, which validates both techniques. Finally, the lists of events are separated into categories based on their properties, including magnitude, frequency, and time of occurrence.

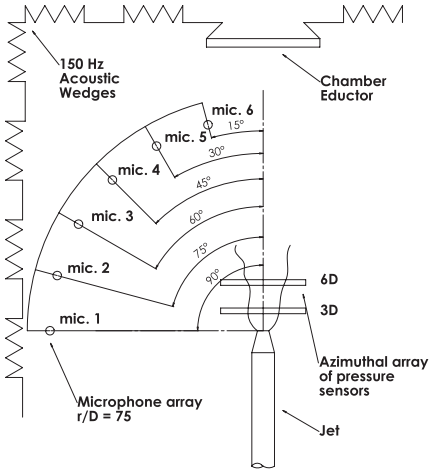

Figure 1. Experimental facilities of jet flow measurement (courtesy K.R. Low).

INTRODUCTION

The noise sources of high speed jet was initially assumed to be random, until the discovery of turbulent coherent structures offered another view to understanding the dynamics. Coherent structures are firstly found to be in part responsible for the occurrence of acoustic spectrum peak (Mollo-Christensen, 1967; Crow and Champagne, 1971). The frequency range associated with the loudest noise was found to be $0.1 < St < 0.7$ (Michalke, 1977). Coherent structures are more amenable to flow control toward noise reduction, and related studies dominate the literature.

The level of coherence was important for jet noise production since a periodic shear layer would not generate far-field noise. Also, it was shown by Michalke and Fuchs (1975) that while the first few azimuthal modes were associated with far-field noise, the axisymmetric mode is not the most efficient. This was related to the coherence level of the velocity field, defined as the ratio of the size of the source to that of the eddies. From the research of Wei and Freund (2006), the more ordered propagation of near-field structures was related with the far-field noise reduction. Cavalieri et al. (2011b) showed that the far-field pressure resulted from the near-field wave packets propagating through a modeled flow field had good correspondence with the experimental data. What we observe in this paper adds to the coherent part of analysis.

DATA DESCRIPTION

In this study, we use two sets of data, one experimental and the other numerical. Our two algorithms, distinct for far-field and near-field processing, are applied to both databases, providing validation of the procedures in spite of the different Mach numbers.

Experimental Data

The experiment was performed in a large-scale (approximately $8000 ft^3$) anechoic chamber in Syracuse University. The data we use for this paper is for a cold jet with Ma = 0.6 and its Reynolds number is 700,000. The top view of the experiment facility is shown in fig. 1. The exit of the nozzle has the diameter of 0.0508m.

To measure far-field pressure, 6 microphones were

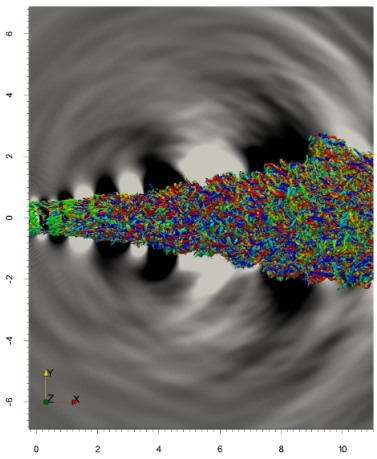

Figure 2. Instantaneous flow visualization of LES data.

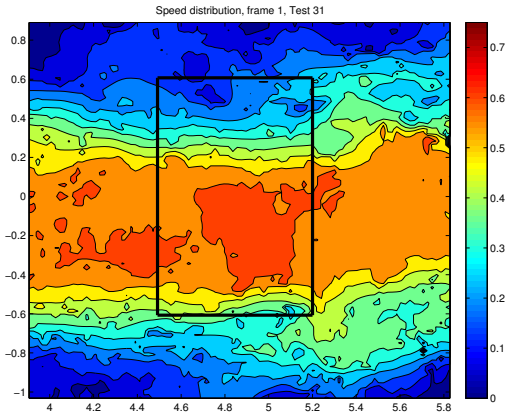

Figure 3. Local instantaneous Mach number (black box is for the region of window averaging).

placed in the same horizontal plane with the jet center line. Their distance from the center of the nozzle is 75 diameters, and they were located in 15^o increments from the jet center. The pressure signals were collected at 40.96 kHz and low-pass filtered at 20.48 kHz. There were 8192 samples for each record. For the algorithm in this paper, we use pressure signal at 15^o microphone.

The near-field 2D velocity field was captured by a 10 kHz TR-PIV simultaneously (Low et al, 2013). 2 cameras with 576 $\times$ 576 pixel resolutions sampled at 20kHz. A Neodym-Yag laser output at 10 kHz in the same horizontal plane of jet centerline and was recorded in 8623 snapshots. A trigger signal was created to ensure the near-field and far-field records were aligned simultaneously. These tests (noted as test 31, 32 and 33) of measurements covered approximately $4 \leq x/D \leq 8$ in the streamwise location and $-1 \leq y/D \leq 1$ in the spanwise. Each test took about 1.5D in the spanwise and had the same transverse locations. The end of the potential core was measured in Test 33, which is counted as the key region of jet noise production.

LES Data

The LES data simulated an isothermal jet with Ma = 0.9 and has the Reynolds number being 400,000. The sampling rate is 80kHz. The numerical algorithm and computation schemes can be found in Daviller (2010), and the details will not be shown here. Fig. 2 is one example of the instantaneous flow field, where the coherent structures are represented by the isosurfaces of Q criterion. The pressure at radial $r/D = 6$ and axial $x/D = 15$ are sampled as far-field signals (D = 0.02 m). For the near-field, the database was filtered to reduce the size by a factor of 3^3. This is applicable at present since we are looking for the relationship between near-field coherent structures and jet noise, which doesn't require the full resolution. Another simplification is the usage of 2D plane instead of full 3D field. The diagnostics listed before are then replicated for the 2D sections.

EXTRACTION OF EVENTS RELATED TO NOISE PRODUCTION

Two independent algorithms will be presented in this section. The first makes use of both near-field velocity field and far-field pressure, after applying cross-correlation, wavelet analysis and pattern recognition scheme, the events that relate near-field and far-field are recorded as 'NF events'. Another algorithm (Lewalle et al., 2012) uses cross-correlation and wavelet analysis as well, however this method focuses on the events that are shared by three far-field microphones and uses no near-field information. The list of 'FF events' thus generated can be interpreted as footprints of near-field sources.

Near-field and Far-field Cross-Correlation

For each NF velocity snapshot, we perform a window averaging (black box in fig. 3) and extract a series of dimensionless statistics. These quantities from successive frames are then recorded respectively in time traces. The statistics include:

- the average speed $< \sqrt{u^2+v^2} >$;
- the absolute value of transverse (radial) component of velocity $<\mid v \mid>$;
- the rms value of $\mid v \mid$;
- the rms value of v;
- the absolute value of Reynolds stress $<\mid uv - < u >< v >\mid>$
- the absolute value large-scale vorticity $<\mid \omega \mid>$;
- the rms value of ω;
- the absolute value of 2-D divergence (trace of rate-of-strain) $<\mid \partial_x u + \partial_y v \mid>$;
- the rms value of $\partial_x u + \partial_y v = s_{xx} + s_{yy}$;
- the absolute value of the determinant of 2-D rate-of-strain $<\mid s_{xx}s_{yy} - s_{xy}^2 \mid>$;
- the rms value of $s_{xx}s_{yy} - s_{xy}^2$.
- the Q criterion $< (||\Omega||^2 - ||S||^2)/2 >=< -\partial_j u_i \partial_i u_j/2 >$;
- the absolute value of Q $<\mid ||\Omega||^2 - ||S||^2 \mid /2 >$;

Looking for the relationship between near-field flow structures and far-field noise, we filtered and down sampled the far-field pressure to match the PIV acquisition rate, and applied cross-correlation and wavelet analysis to the diagnostics and pressure signals.

The cross-correlation reaches the maximum at the lag that corresponds to acoustic propagation time (fig. 4). The time of sound propagation is estimated by dividing the Cartesian distance by ambient speed of sound, resulting in a typical 10.5 ms expected lag between NF and FF. As the distance decreases (from top row to bottom row), it can be observed in fig. 4 the corresponding reduction of lags.

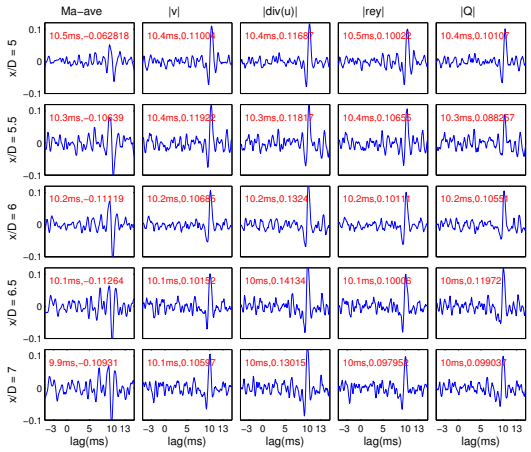

Figure 4. Cross-correlation of NF diagnostics and FF signals in the time domain (PIV data).

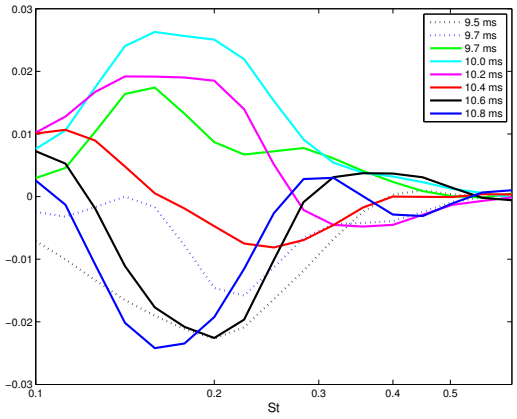

Figure 5. Variation of cross-correlation of 2D divergence and FF signals v.s. frequency (PIV data).

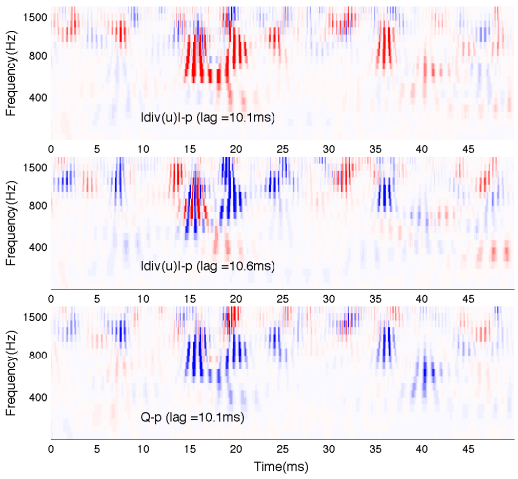

Figure 6. Contributions to cross-correlation in TFL domain; red is positive, blue negative.

The largest value of peak cross-correlation appears roughly around $x/D = 6.5$, which is near the end of potential core. All the diagnostics show the pattern described above, and this can be interpreted as the occurrence of yet-unknown events influencing all these quantities in conjunction with the noise production observed from the far-field.

These cross-correlations are resolved in frequency. Taking the real part of the Morlet wavelet transform provides the narrow-band frequency resolution of the cross-correlations. The formula below defines the transformed coefficient of near-field signals in time-frequency domain.

$$NF_M(t,\omega) = \int NF(t+t')\psi_M(\omega t')dt'. \qquad (1)$$

Similarly the transformation of far-field pressure $FF_M(t,\omega)$ can be obtained. Then we can calculate the cross-correlation in time-frequency domain by correlating at each frequency level:

$$\rho(\tau,\omega) = \int NF_M(t,\omega)\, FF_M(t+\tau,\omega)\, dt. \qquad (2)$$

Two different normalizations are compared during this process. One is to normalize the filtered signals to unit variance and then correlate them. The resulted filtered correlation level reaches 30% to 40%. This method factors out the energy information and makes the low-frequency event stand out (below Strouhal 0.1). The other correlates the signals without normalization (fig. 5). The frequency range of around Strouhal 0.2 becomes dominant, which is also that of peak of energy spectrum. Focusing on the events that offer more obvious physical interpretation for the present, we are using the second normalization for the remaining content. Different diagnostics again generate very similar figures. Some difference exists in the sign of the peak correlation, which is caused by the in-phase or out-of-phase state of the two compared signals. LES dataset gives very similar patterns, with a shift towards higher frequency, which may be caused by the higher Mach number.

Pattern Recognition of Individual Wave Packets Moving from the statistical to the event level, we use a pattern recognition scheme to extract the contributions of correlation in time and frequency domain. Morlet wavelet is again applied to the near- and far-field signals and the real part of the transformation coefficients are correlated without averaging in frequency levels (fig. 6). The strong red or blue patches represent the main correlation contributors where the signals are locally in phase or half a period out of phase. The oscillations, e.g., at $15 < t < 17ms$, can be viewed as short wave packets in the time domain. The first two frames show the phase shift of half a period as we change the lags. Different diagnostics share a lot of common patterns (e.g. last frame).

Viewing the highly correlated red or blue patches as noise-related events, we tested for false positives resulting from the chance occurrence of such patches. Indeed, any unstructured signal, when band-pass filtered, will contain local oscillations. The correlation contour plots of white Gaussian noise and of incorrectly-lagged (i.e. presumably independent) signals look very similar to fig. 6. However, the patches are as likely to be positive as negative at every frequency level and they tend to cancel out when averaged; the incomplete cancellation for our finite record length gives residual correlations of the order of 3 to 5%, well below the

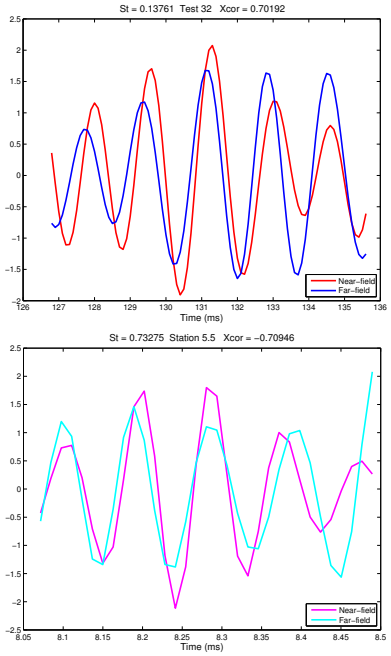

Figure 7. Matched events between near- and far-field (1st frame for PIV and the other for LES data).

10 to 20% level observed for the actual signals and the 25 to 35% level calculated with frequency resolution. While the list of events obtained below will unavoidably contain some false positives, the large majority of them cannot be due to chance.

The local extrema of these instantaneous contributions are collected over a range of lags oscillating approximately 1 period from that of peak cross-correlation. We extracted the envelopes of the packets of oscillations as in Fig. 6. Around the local peak value, we extracted a few periods and calculated the excerpts' cross-correlation between NF and FF. The event is added to the list if the excerpt correlation coefficient exceeds 0.6, and if the far-field magnitude is at least twice the mean value. This ensures that the recorded events are strong enough to be physically important. Fig. 7 shows two examples of the resulting excerpts, one from PIV and the other from LES data.

In order to get some statistical level description of the NF events, we collect the events recognized by all the diagnostics and keep those that are common to at least two of them. About 250 out of 450 excerpts (about 60%) are kept in this final list and they will be referred to as NF events in this paper. Their distribution and property histogram is shown in fig. 8. In the scattering plot, the x-positions of the markers are shifted randomly from the original (within 20%) to alleviate the overlap. The magnitude vs. frequency distribution resembles that of energy spectrum. The lower frame shows the 2D histogram of number of events at different frequency and magnitude levels. The darkest spot, representing the majority of the events are clustered around Strouhal 0.2.

Far-field Pressure Signatures of Individual Noise Sources

The far-field acoustic signals contain the distorted signature of individual coherent near-field sources. The 15^o, 30^o and 45^o far-field microphones are within the cone of co-

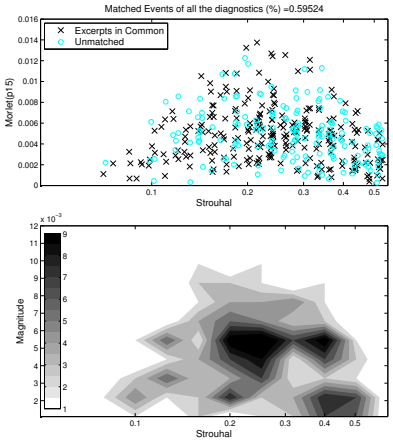

Figure 8. a. Distribution matched and unmatched events; b. Property histogram of matched events.

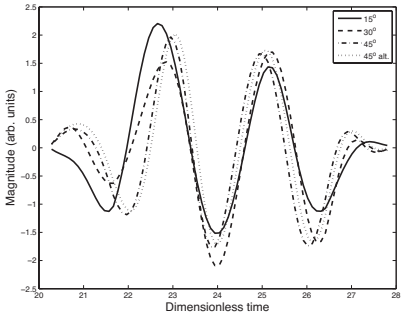

Figure 9. Matched events at 15^o, 30^o, 45^o microphones.

herence and are used to identify some of the loudest events. Detailed algorithm description can be found in Lewalle et al. (2012). Since 15^o pressure has the most dominant coherent noise of the three, we make a list of local maxima of its Morlet coefficients. These are the loudest events captured by this microphone. Then we keep three periods of the Mexican hat coefficients centering at each of these loud events. These short signals are then correlated with their corresponding parts from the other two microphones. This provides the lags between microphones for the events. If the peak value of $15-30^o$ cross-correlation is above 0.75, and that of $15-45^o$ exceeds 0.35, with its corresponding largest lag not bigger than 35 time steps, we keep this as one FF event (one example shown in fig. 9). We verified that the list of FF events is not affected by the down-sampling to 10kHz.

COMPARISON OF NF EVENTS AND FF EVENTS

Three levels of comparison of the FF and NF approaches are possible: statistical (using the entire length of the available records), local (on an event-by-event basis), and collective (comparing the populations of events, which amounts to conditional statistics). We will address firstly the statistical and collective level and then perform the event-by-event comparison.

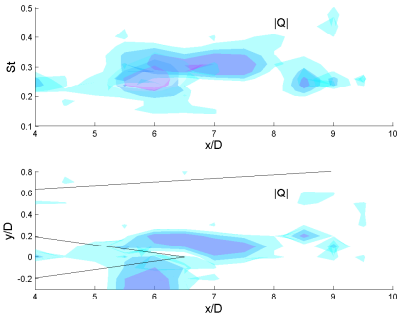

Figure 10. Distribution of peak cross-correlation contributions between Q (pressure source term) and far-field pressure.

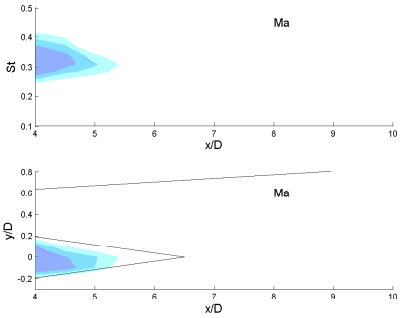

Figure 12. Distribution of peak cross-correlation contributions between Ma and far-field pressure.

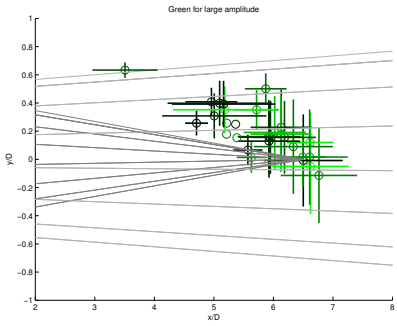

Figure 11. Location of sources obtained from the far-field cross-correlation algorithm (LES data) and triangulation to the near-field.

Distribution in Space/Frequency

The statistical results are resolved according to streamwise and transverse location and according to frequency. For a given diagnostic, we can plot the contributions to cross-correlation with the far-field, as a percentage of the largest value for this diagnostic. The most active regions are mapped out as iso-surfaces of constant relative contribution to the cross-correlation, in the (x-y-St) coordinates. The result for Q is shown in fig. 10, for the LES data. Iso-surfaces for levels 50, 65 and 80% of maximum are superposed and the color scale is from cyan to magenta for weaker to stronger levels. In addition to being a topological index, Q is also proportional to the source term in the incompressible pressure equation $\nabla^2 p = -\frac{Q}{\rho}$. Thus large correlation of Q with the far-field pressure is indicative of actual production of far-field noise. We see that this active region is located primarily in the shear layer, close to the centerline near the tip of the potential core at $5.5 < x/D < 7.5$, with some residual activity farther downstream. The corresponding Strouhal number is in the vicinity of 0.3, matching the peak of the far-field acoustic spectrum.

This statistical result agrees closely with the estimates of source location obtained by triangulation from the FF events, as shown in fig. 11. The algorithm for triangulation is based on the small differences in detection times at 4 far field (numerical) microphones, which corresponds to differences in distance between source and microphone. The error bars cover the source locations that give similar integer values of the lags at the available sampling rate of 80 kHz. We conclude that the FF events and NF correlations concur about the location of the sources of noise.

The statistical picture differentiates between diagnostics. Velocity-derivative diagnostics tend to agree with the Q results shown above, with some additional activity at $8 < x/D < 10$ which is tentatively interpreted as the turbulent aftermath of the noise production. However, velocity-based diagnostics paint a different picture. For example, the local Mach number (dimensionless speed) is correlated to far-field pressure mostly inside the potential core itself, as seen in Fig. 12. The physical interpretation of this correlation is the subject of on-going work.

Comparison of Lists of Events and Some Statistics

From the two independent algorithms described above, we get two lists of events. Their excerpts, illustrated in fig. 9 for FF and fig. 7 for NF, are observed as short wave packets, which appear consistent with Cavalieri et al (2011a).

- 'FF events' that are captured by 3 far-field microphones. These events are energetic and cluster near the acoustic peak. They oscillate for 3 to 5 periods, making a form of wave packets, even though the identification algorithm uses Mexican hat wavelet and does not presuppose an oscillatory pattern. The list consists of about 260 events.
- 'NF events' that are common to near-field kinematics and far-field acoustics (15^o microphone only). These events are the connection between near-field and far-field but are not necessarily the loudest ones. This list has about 150 events.

To find the matches between these two lists of events, we construct the following criteria: the time of occurrence of two events are within one period of each other, the frequencies are within a factor of $\sqrt{2}$ of each other, and their magnitudes of filtered far-field pressure coefficient are less than 25% apart on their respective scales. The last criteria is to make sure the very loud event is not too weak in the other. With these being set, nearly 60% are found in common. The same algorithm is tested by replacing the far-field signal by White Gaussian noise or incorrectly lagged signals. This yields only about 10% in common. Therefore it may be concluded that these two independent algorithms identify many of the same events. This is also verification of both of the algorithms.

The distribution and histograms of the matched and unmatched events can be found in fig. 13. The majority of the matched events have frequency of about Strouhal 0.2 to 0.3

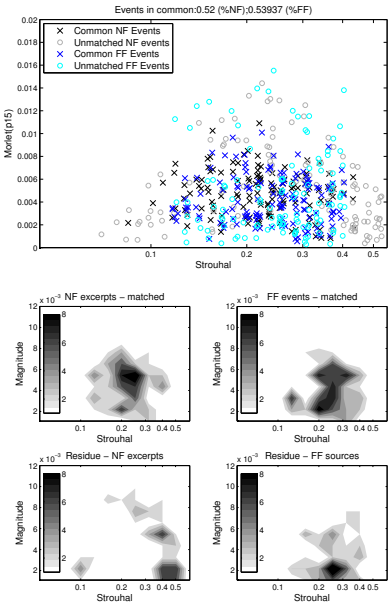

Figure 13. Distribution and property histograms of matched and unmatched events.

and show some difference in magnitude that is allowed by the flexibility of matching algorithm. The unmatched events are either too high or too low in frequency as NF events and have very low magnitude as FF events.

DISCUSSION

The connection between near-field kinematics and far-field acoustics of high speed jets has been observed in both statistical and event level. Allowing for chance matches, the interpretation of events as source-related is supported by the large correlation coefficients. The large portion of similarity between the results of two independent algorithms, which is also high above the chance level, is another verification of the relationship between extracted events to noise sources.

The FF events that are common to three far-field microphones signals display pattern of wave packets. For the NF events, the wave packet shape may be an artifact of the Morlet wavelet. But since this list shares about 50% of the events with the former, it is reasonable to state that this list of events also takes the wave packet form. Our algorithm generates very similar results for both experimental and LES dataset, which helps to verify the reliability of the scheme.

Although the diagnostics display a lot of common features, some difference between velocity-related and velocity-derivative-related diagnostics is emerging. Fig. 14 compares the diagnostics one by one. The RMS values are not compared here since they are more like their original values (70% in common on average). This is consistent with our previous analysis (fig. 10). These two combinations seem to leads to two different populations of events which capture different flow structures.

Some aspects that we would like to look further into include: look at the PIV snapshots and try and identify the mechanism of noise production; the portion of events that are highly correlated between NF and FF but with unexpected low frequency needs to be understood further; it is also surprising that about a dozen diagnostics show correlation to the far-field and their similarities and differences will be investigated. We will also make use of the near-field pressure information in future research.

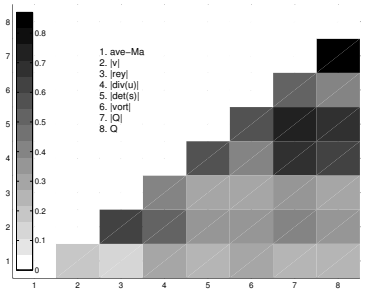

Figure 14. Percentage of matched events of 2-diagnostic combinations.

This work was supported in part by a AFOSR grant, Spectral Energies, a Syracuse University Graduate Fellowship and by an SU Research Growth Award of Mechanical Department. We are indebted to the members of the Glauser group at SU for the data acquisition and processing and many discussions, particularly with Mark Glauser, Kerwin Low, Patrick Shea and Zach Berger; and at Pprime with Bernd Noack, Peter Jordan, Joel Delville and Jean-Paul Bonnet. Several SU undergraduate students, G. Freedland, A. Tenney and V. Holcomb, participated in verification of some of the algorithms.

REFERENCE

Cavalieri, A., Daviller, G., Comlte, P., Jordan, P., Tadmor, G. and Gervais, Y. 2011a, "Using large eddy simulation to explore sound-source mechanisms in jets", *J. Sound Vib.*, 330, 40984113.

Cavalieri, A. V. G., Jordan, P., Agarwal, A. and Gervais, Y., 2011b, "Jittering wave-packet models for subsonic jet noise", *J. Sound Vib.* 330, 44744492.

Crow, S. C. and Champagne, F. H., 1971, "Orderly structure of jet turbulence", *J. Fluid Mech.* 48, 547591.

Daviller, G., 2010, "Numerical study of temperature effects in round and coaxial jets", PhD thesis, Ecole Nationale Sup erieure de M ecanique et dA erotechnique, Poitiers, France.

Lewalle, J., Low, K. R. and Glauser, M. N., 2012, "Properties of the far-field pressure signatures of individual jet noise sources", *Int. J. Aeroacoustics*, 11, 651 674.

Low, K. R., Berger, Z. P., Kostka, S., ElHadidi, B., Gogineni, S. and Glauser, M. N., 2013, "A low-dimensional approach to close-loop control of a mach 0.6 jet", *Exp. Fluids*, 54, 117.

Michalke, A., 1977, "On the effect of spatial source coherence on the radiation of jet noise", *J. Sound Vib.* 55, 377394.

Michalke, A. and Fuchs, H. V., 1975, "On turbulence and noise in an axisymmetric shear flow", *J. Fluid Mech.* 70, 179205.

Mollo-Christensen, E., 1967, "Jet noise and shear flow instability seen from an experimenters viewpoint", *J. Appl. Mech.* 34, 17.

Wei, M. and Freund, J. B., 2006, "A noise-controlled free shear flow", *J. Fluid Mech.* 546, 123152.